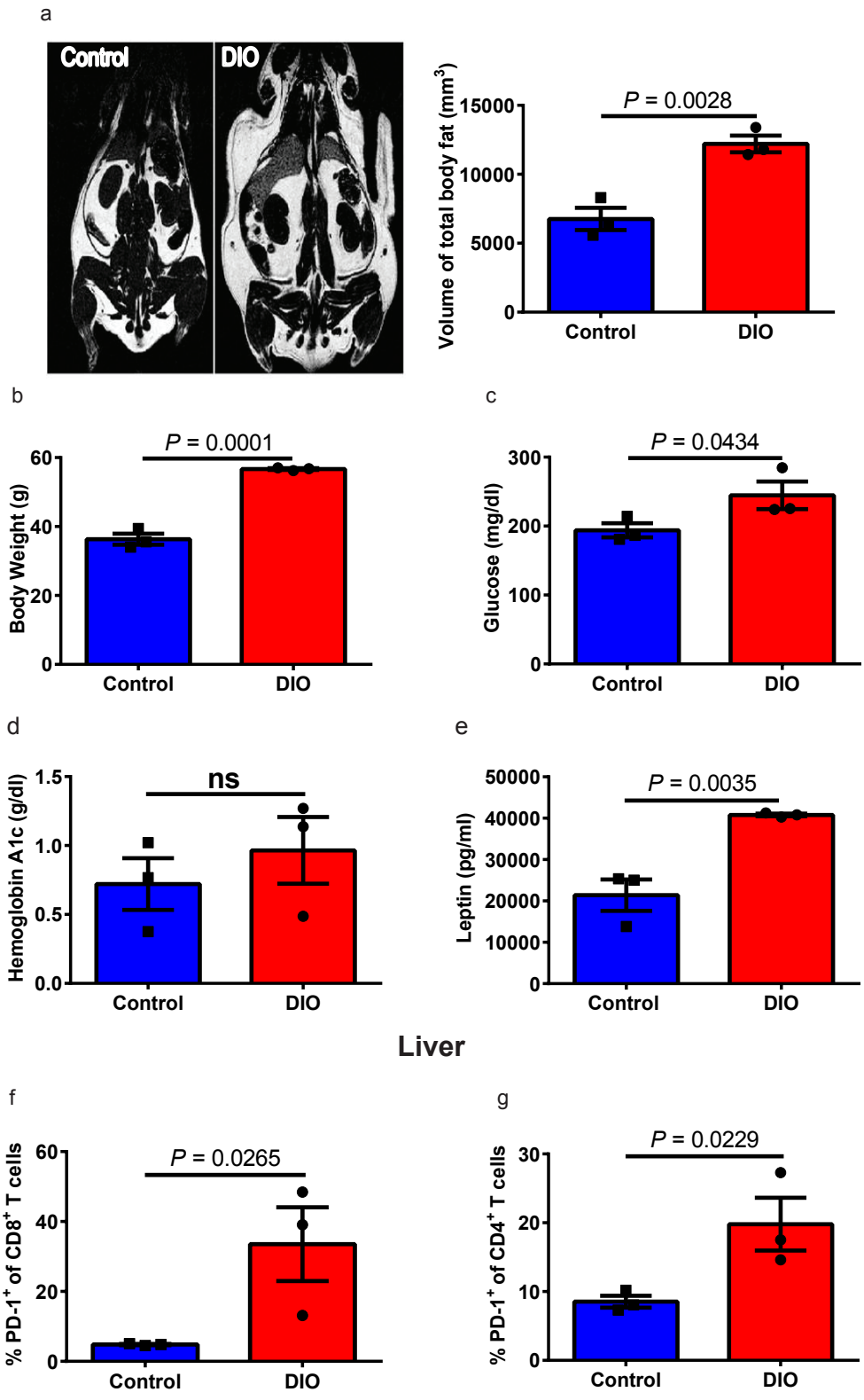


**Supplementary Figure 1: Phenotypes of 6-month-old male control and DIO mice.** a) Body (subcutaneous and visceral) fat of mice quantified by T1-weighted MRI scans (n=3/group). b) Body weights (n=3/group), serum c) glucose (n=3/group), d) HbA1c (n=3/group), and e) leptin levels (n=3/group). PD-1 expression of f) CD8+ and g) CD4+ T cells in the liver assessed by flow cytometry (n=3/group). Data in this figure are all depicted as mean ±s.e.m., with all individual points shown. One-tailed unpaired Student's t-test p-values shown.

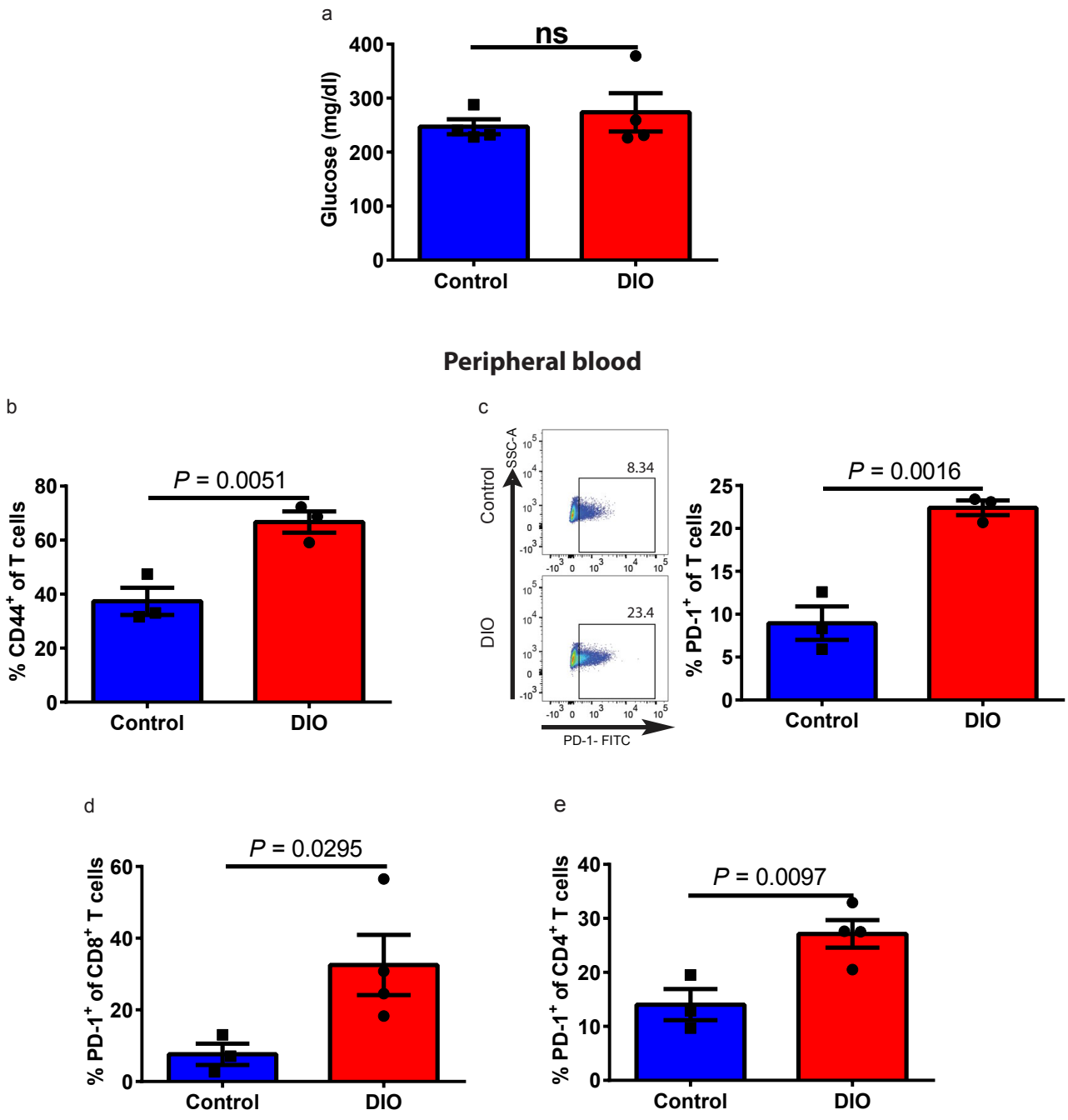


**Supplementary Figure 2: Phenotypes of 11-12-month-old male control and DIO mice.** a) Serum glucose levels (n=4/group). b) Frequency of CD44+ T cells in the peripheral blood (n=3/group). c) Representative flow plots and frequency of PD-1+ T cell in the peripheral blood (n=3/group). PD-1 expression on peripheral blood d) CD8+ and e) CD4+ T cells (n=3 in control group, n=4 in DIO group). Data in this figure are all depicted as mean ±s.e.m., with all individual points shown. One-tailed unpaired Student's t-test p-values shown.

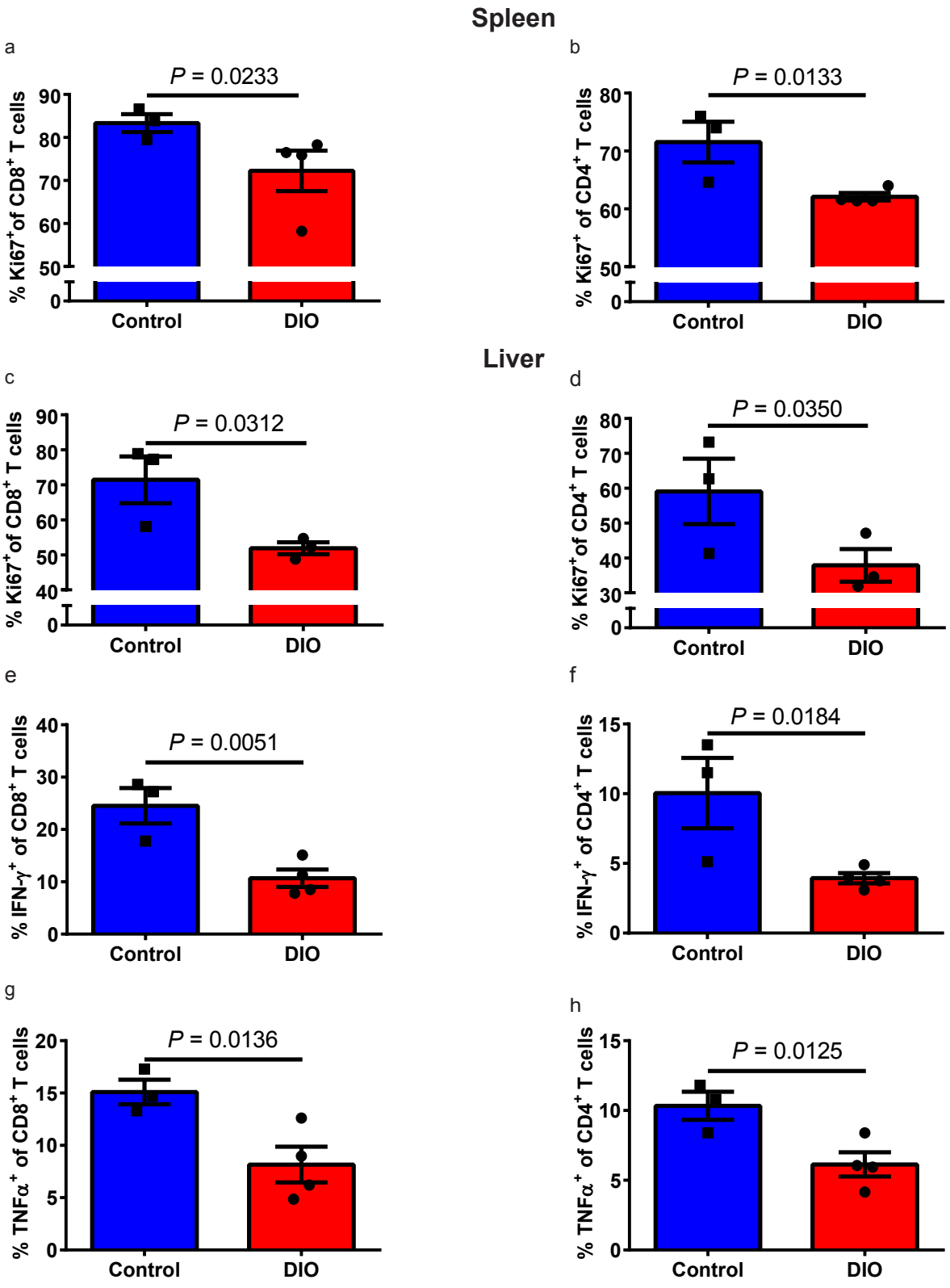


**Supplementary Figure 3: T cell functions of 11-12-month-old male control and DIO mice.** Ki67 expression on a) CD8+ and b) CD4+ T cells in the spleen after ex vivo stimulation (n=3 in control group, n=4 in DIO group). Ki67 expression on c) CD8+ and d) CD4+ T cells in the liver after ex vivo stimulation (n=3/group). e-f) IFNγ, and g-h) TNFα production on CD8+ and CD4+ T cells in the liver after ex vivo stimulation (n=3 in control group, n=4 in DIO group). Data in this figure are all depicted as mean ±s.e.m., with all individual points shown. One-tailed unpaired Student's t-test p-values shown

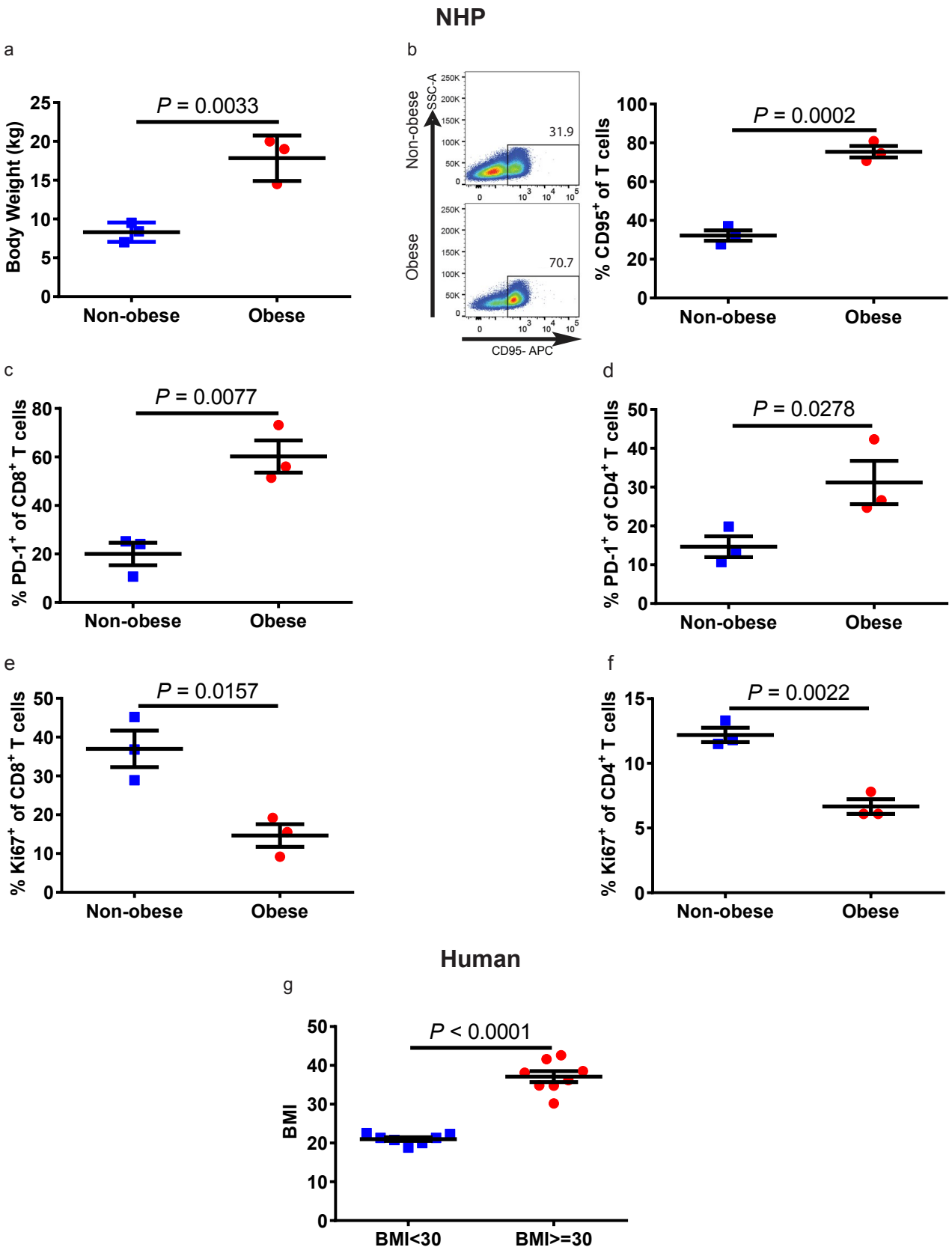


**Supplementary Figure 4: Phenotypes of non-obese vs. obese higher species.** a) Body weights of non-obese and obese rhesus macaques (n=3/group). b) Representative flow plots and frequency of CD95+ T cells in the peripheral blood of non-obese and obese rhesus macaques (n=3/group). PD-1 expression on c) CD8+ and d) CD4+ T cells in the peripheral blood of rhesus macaques (n=3/group). Ki67 expression on e) CD8+ and f) CD4+ T cells after ex vivo stimulation of non-obese and obese rhesus macaque PBMCs. g) BMI of non-obese (BMI<30, n=7) and obese (BMI>30, n=8) human healthy volunteers. Data in this figure are all depicted as mean ±s.e.m., with all individual points shown. One-tailed unpaired Student's t-test p-values shown.

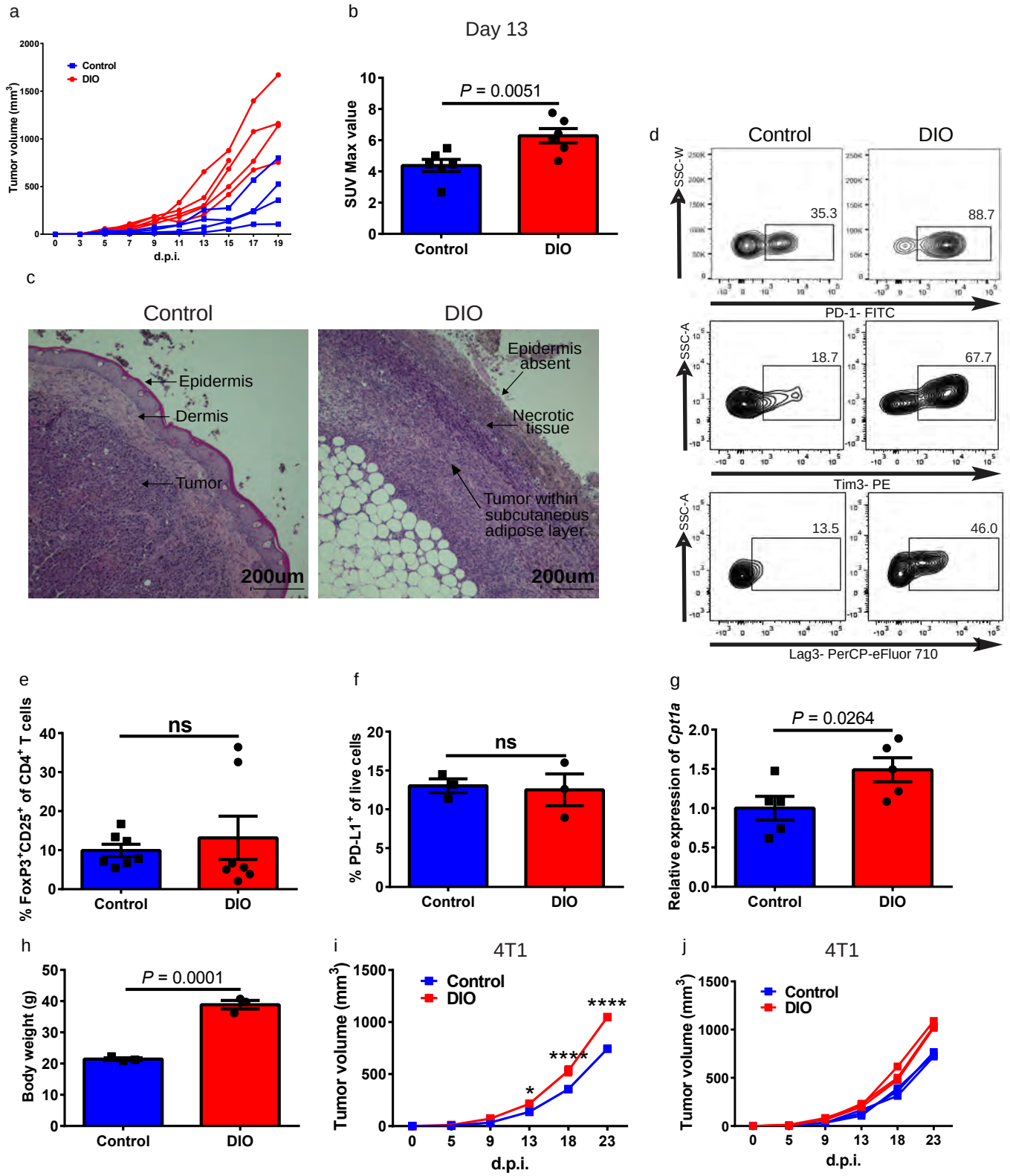


**Supplementary Figure 5: Phenotypes of tumor-bearing control and DIO mice.** a) Individual tumor volumes of B16 melanoma in 6-month-old control (n=4) and DIO (n=5) C57BL/6 male mice. b) Quantification of tumor burden by PET-CT imaging of 6-month-old B16-F0-tumor-bearing control and DIO (n=6/group) mice 13 d.p.i. c) Representative H&E staining of tumors from 6-month-old control and DIO B16-F0-bearing male mice. d) Representative flow staining of PD-1, Tim3, and Lag3 on tumor infiltrating CD8+ T cells from 6-month-old B16-bearing control and DIO male mice at 16 d.p.i. Frequency of e) T regulatory (FoxP3+CD25+CD4+) cells (n=7/group) and PD-L1+ cells (n=3/group) in the B16-F0 tumors from 6-month-old control and DIO male mice. g) The relative expression of *Cpt1a* in the tumors from 6-month-old B16-bearing control and DIO male mice (n=5/group). h) Body weights of 6-month-old control and DIO female BALB/c mice (n=3/group). b, e-h) Data are depicted as mean ±s.e.m., with all individual points shown. One-tailed unpaired Student's t-test p-values shown. i) Tumor volume of 4T1 inoculated orthotopically in 6-month-old control and DIO female BALB/c mice (n=3/group). Tumor volumes are depicted as mean ±s.e.m. Two-way ANOVA with Tukey post-hoc test used to compare groups. j) Individual tumor volume of 4T1 tumors in 6-month-old control and DIO female BALB/c mice (n=3/group). *p<0.05, **** p<0.001.

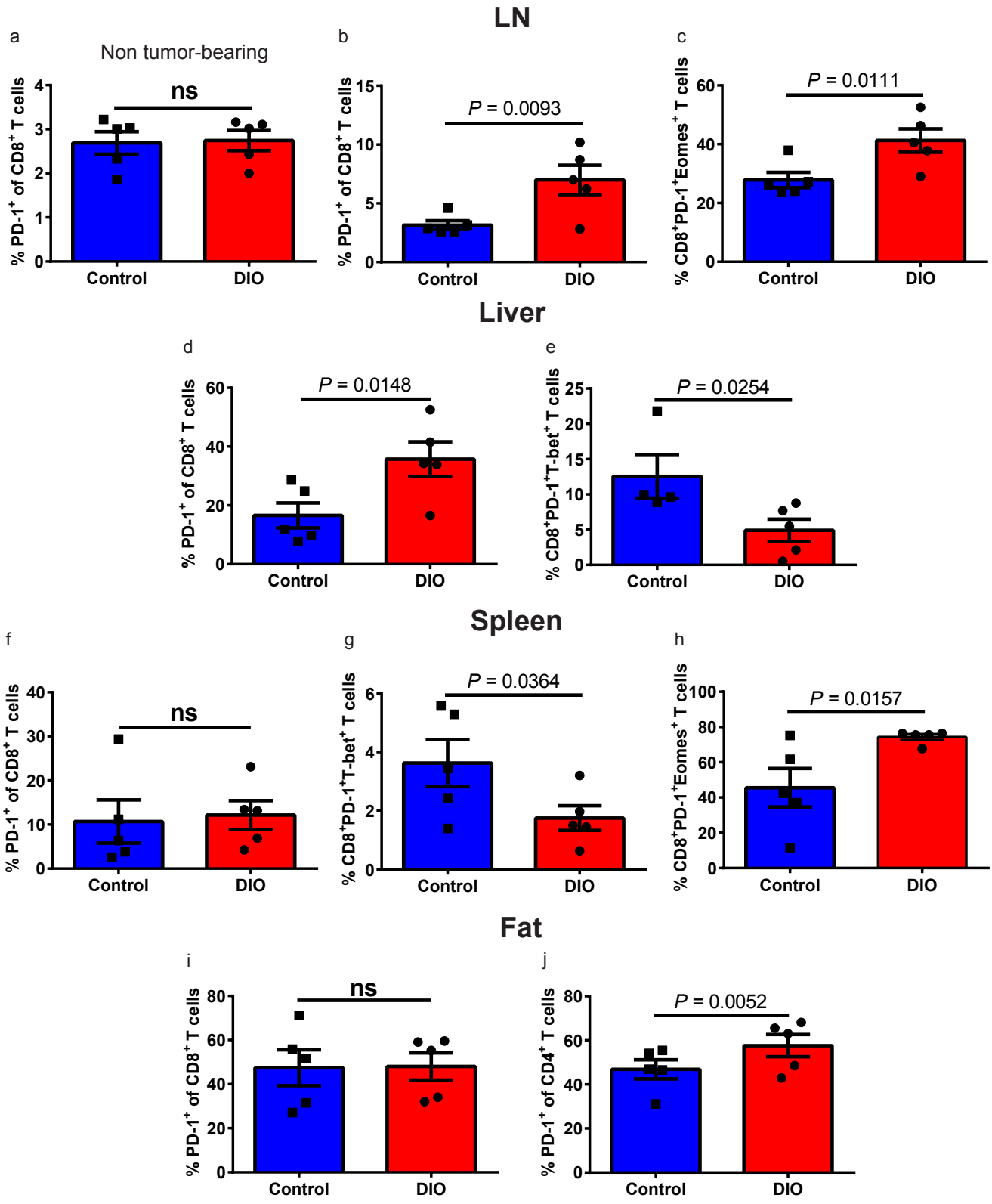


**Supplementary Figure 6: Obesity promotes T cell exhaustion systemically during tumor progression.** Frequency of PD-1 on CD8+ T cells from the inguinal LN of 6-month-old a) non-tumor-bearing and b) B16-F0-bearing control and DIO mice (n=5/group). Frequency of Eomes on PD-1+CD8+ T cells from c) draining LN and h) spleens of 6-month-old B16-F0 bearing control and DIO mice (n=5/group). Frequency of PD-1 on CD8+ T cells from the d) liver and f) spleen of 6-month-old B16-F0-bearing control and DIO mice (n=5/group). Frequency of T-bet on PD-1+CD8+ T cells from the e) liver (n=4 in control group, n=5 in DIO group) and g) spleen (n=5/group) of 6-month-old B16-F0-bearing control and DIO mice. Frequency of PD-1 on i) CD8+ and j) CD4+ T cells from the fat of 6-month-old B16-F0-bearing control and DIO mice (n=5/group). Data in this figure are all depicted as mean ±s.e.m., with all individual points shown. One-tailed unpaired Student's t-test p-values shown.

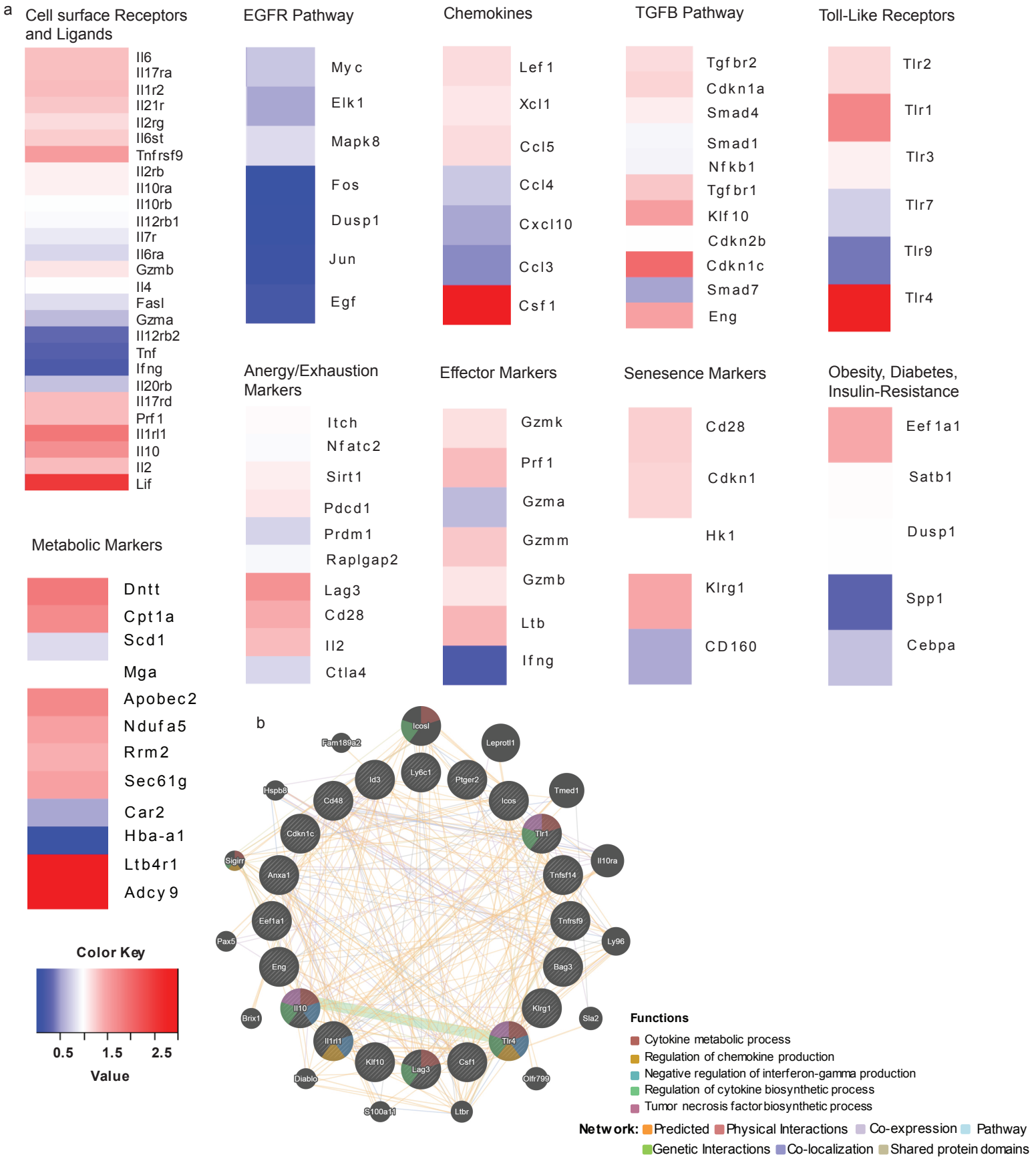


**Supplementary Figure 7: Differential gene expression and network analysis on memory CD8+ T cells from tumor-bearing control and DIO mice.** a) Heat maps showing differentially expressed gene clusters (>1.5 fold) and b) network analysis of up-regulated genes from enriched gene sets (using GeneMANIA) in CD8+CD44+ T cells isolated from the spleens and lymph nodes of 6-month-old control or DIO mice bearing B16-F0 at 16 d.p.i. Data shown as fold change of DIO over control.

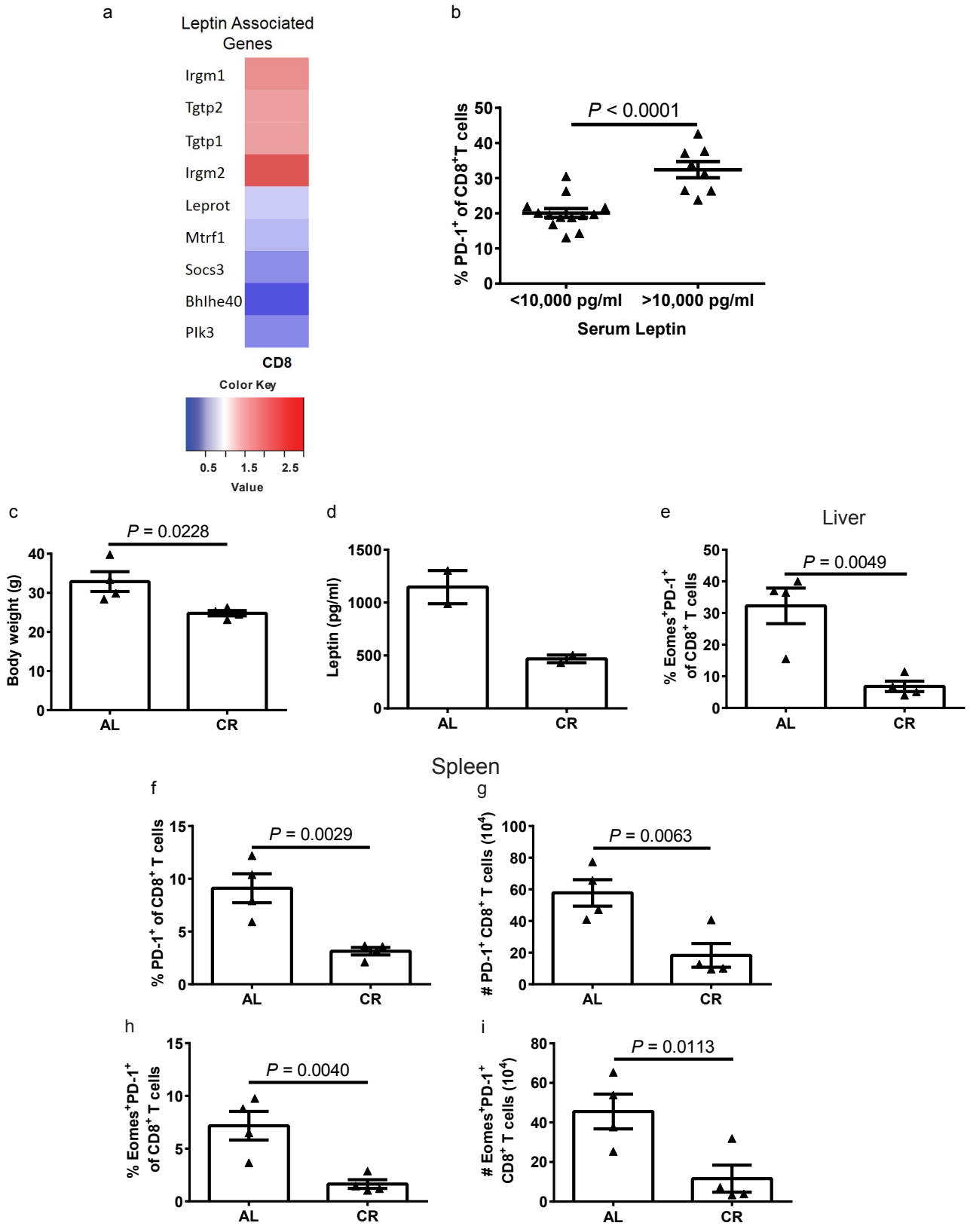


**Supplementary Figure 8: The correlation of leptin level with immune exhaustion profiles.** a) Heat maps showing differentially expressed leptin-associated genes (≥1.5-fold difference) in CD44+CD8+ T cells isolated from the spleens and lymph nodes of 6-month-old B16-F0-bearing control and DIO C57BL/6 male mice at 16 d.p.i. (data shown as fold change over controls) (n=3/group). b) Frequency of PD-1 expression on CD8+ T cells in the peripheral blood of low (<10,000 pg/ml, n=13) and high (>10,000 pg/ml, n=8) serum leptin cohorts of human healthy volunteers. c) Body weight (n=4/group) and d) leptin levels (n=2/group) of 19-month-old AL and CR male mice. e) Frequency of Eomes expression on liver PD-1+CD8+ T cells of 19-month-old AL and CR male mice (n=4/group). f) Frequency and g) total number of PD-1+CD8+ splenic T cells in AL and CR mice (n=4/group). h) Frequency and i) total number of Eomes+PD-1+CD8+ splenic T cells in AL and CR mice (n=4/group). Data in this figure are all depicted as mean ±s.e.m., with all individual points shown. One-tailed unpaired Student's t-test p-values shown.

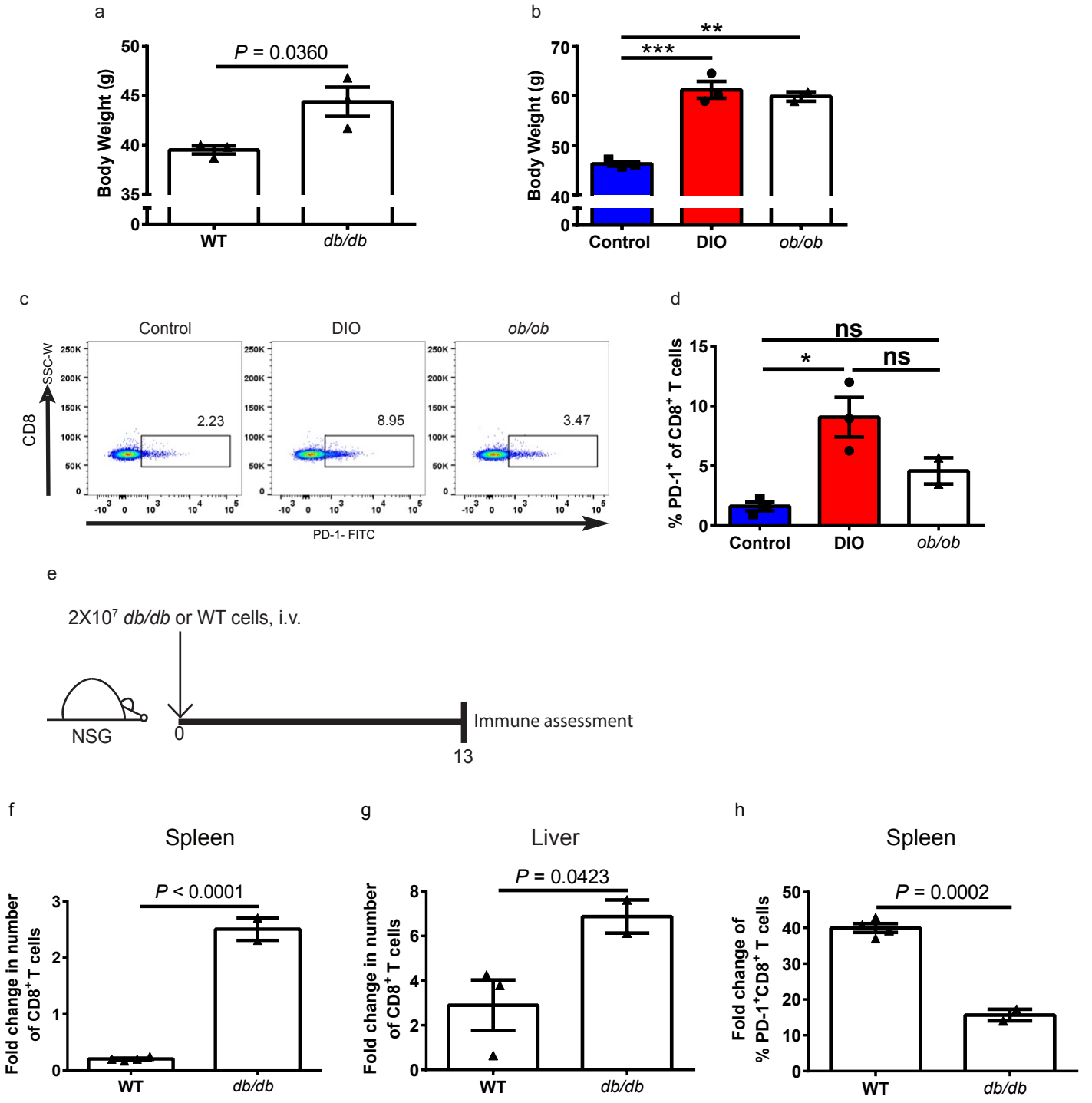


**Supplementary Figure 9: The lack of leptin signaling is associated with decreased T cell dysfunction.** a) Body weights of age-matched (9-month-old) control and *db/db* male mice (n=3/group). b) Body weights of age-matched control (n=3) and DIO (n=3) mice and weight-matched *ob/ob* (n=2) mice. c) Representative flow plots and d) frequency of PD-1ex-pression on splenic T cells of age-matched control (n=3) and DIO (n=3) mice and weight-matched *ob/ob* (n=2) mice. Data are depicted as mean ±s.e.m., with all individual points shown. One-way ANOVA with Tukey post-hoc test used to com-pare groups *p<0.05, ***p<0.001. e) Schema of adoptive transfer of cells from spleens and LNs of WT and *db/db* mice into NSG mice. The fold change of WT or *db/db* CD8+ T cells transferred into NSG mice versus the number f) in the spleen (n=4 in WT group, n=2 in *db/db* group), and g) in the liver (n=3 in WT group, n=2 in *db/db* group) at 13 days post-transfer. h) Fold change in PD-1 expression on splenic CD8+ T cells of NSG mice prior to versus 13 days post-transfer (n=4 in WT group, n=2 in *db/db* group). a, f-h) Data are depicted as mean ±s.e.m., with all individual points shown. One-tailed unpaired Student's t-test p-values shown.

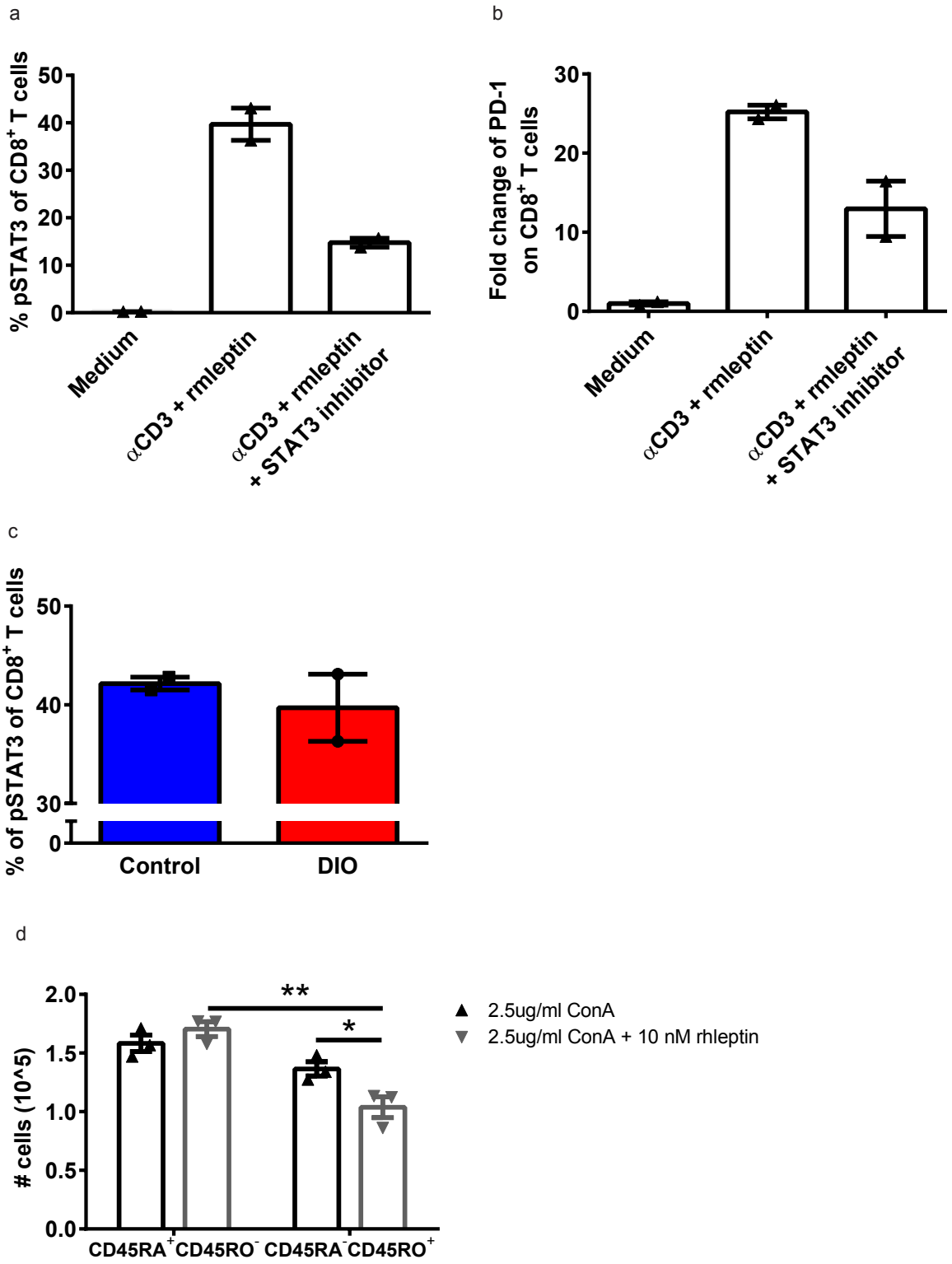


**Supplementary Figure 10: Leptin effects on T cell function in vitro.** a) Frequency of pSTAT3 and b) fold change of PD-1 on splenic CD8+ T cells cultured with αCD3 + rmleptin, αCD3 + rmleptin and STAT3 inhibitor, or medium only for 24 hrs (n=2 technical replicates). c) Frequency of pSTAT3 on splenic CD8+ T cells stimulated with αCD3+ rmleptin for 24 hrs (n=2 technical replicates). d) Total number of sorted naïve (CD45RA+CD45RO-) and memory (CD45RA-CD45RO+) T cells from human PBMCs after stimulation by ConA with or without the addition of rhleptin (n=3 technical replicates). Data are depicted as mean ±s.e.m., with all individual points shown. One-tailed unpaired Student's t-test *p<0.05, **p<0.01.

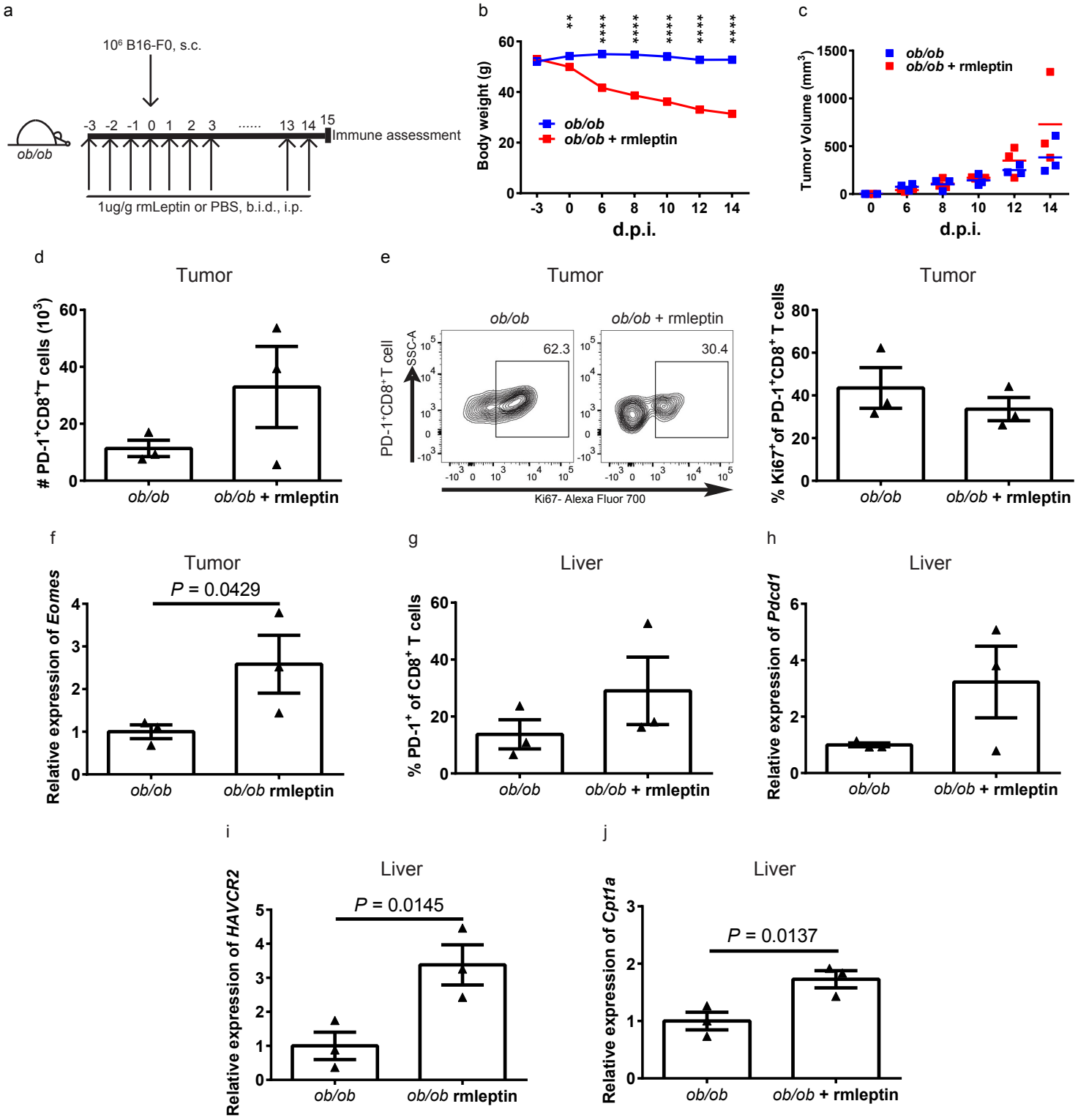


**Supplementary Figure 11: Exogenous leptin promotes T cell exhaustion in vivo.** a) Schema of tumor implantation and rmleptin treatment in *ob/ob* mice. b) Body weight of 3-month-old *ob/ob* male mice bearing B16-F0 treated with or without rmleptin. Data are depicted as mean ±s.e.m. Two-way ANOVA with Tukey post-hoc test used to compare groups. c) Tumor volumes of 3-month-old ob/ob male mice bearing B16-F0 treated with or without rmleptin. Data are depicted as mean+individual volumes (n=3/group). d) Total number of PD-1+CD8+ T cells and e) representative flow plot and frequency of Ki67+PD-1+CD8+ T cells in the B16-F0 tumors of *ob/ob* mice with and without rmleptin treatment. f) The relative expression of *Eomes* in the tumor of B16-F0-bearing *ob/ob* mice with and without rmleptin treatment. g) Frequency of PD-1+CD8+ T cells and the relative expression of h) *Pdcd1*, i) *HAVCR2*, and j) *Cpt1a* in the livers of B16-F0-bearing *ob/ob* mice with and without rmleptin treatment. d-j) Data are depicted as mean ±s.e.m., with all individual points shown. One-tailed unpaired Student's t-test p-values shown.

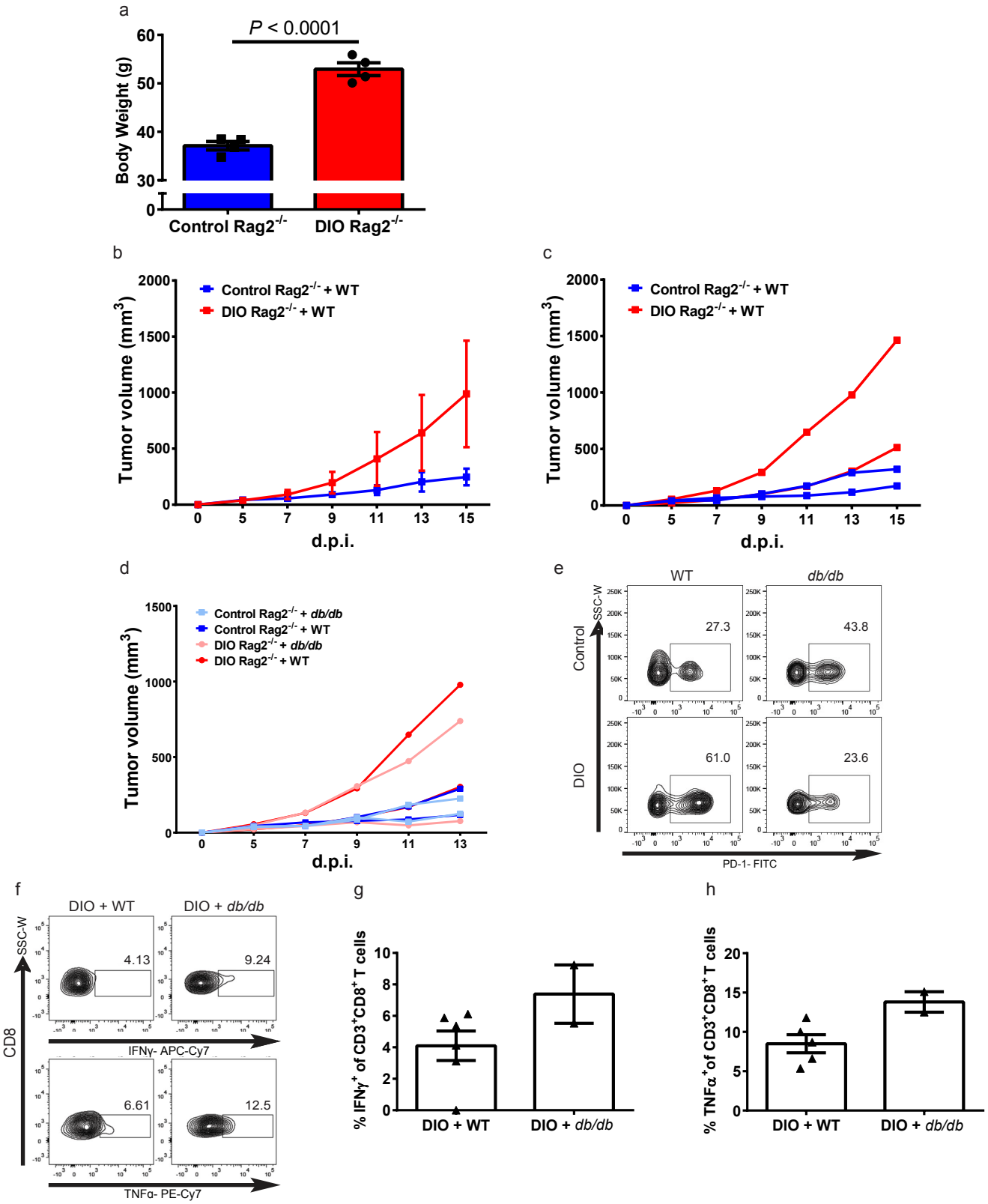


**Supplementary Figure 12: The lack of leptin signaling prevents T cell exhaustion mediated tumor progression in DIO mice.** a) Body weights of 5-month-old control and DIO C57BL/6 Rag2-/- male mice (n=4/group). Data are depicted as mean ±s.e.m., with all individual points shown. One-tailed unpaired Student's t-test p-value shown. b) Tumor volumes and c) individual tumor volumes following B16-F0 subcutaneous inoculation in 5-month-old control and DIO Rag2-/- mice with adoptively transferred WT T cells. d) Individual B16-F0 tumor growth in control and DIO Rag2-/- mice after adoptive transfer of T cells from either WT or *db/db* C57BL/6 mice. e) Representative flow plots of PD-1 on tumor infiltrating CD8+ T cells from B16-F0-bearing control and DIO Rag2-/- mice with adoptive transfer of T cells from either WT or *db/db* C57BL/6 mice. f) Representative flow staining and frequency of g) IFNγ and h) TNFα on adoptively transferred WT and *db/db* CD8+ T cells from the tumors of B16-F0-bearing DIO Rag2-/- mice after ex vivo stimulation (n=2/group, 2-3 technical replicates in WT group).

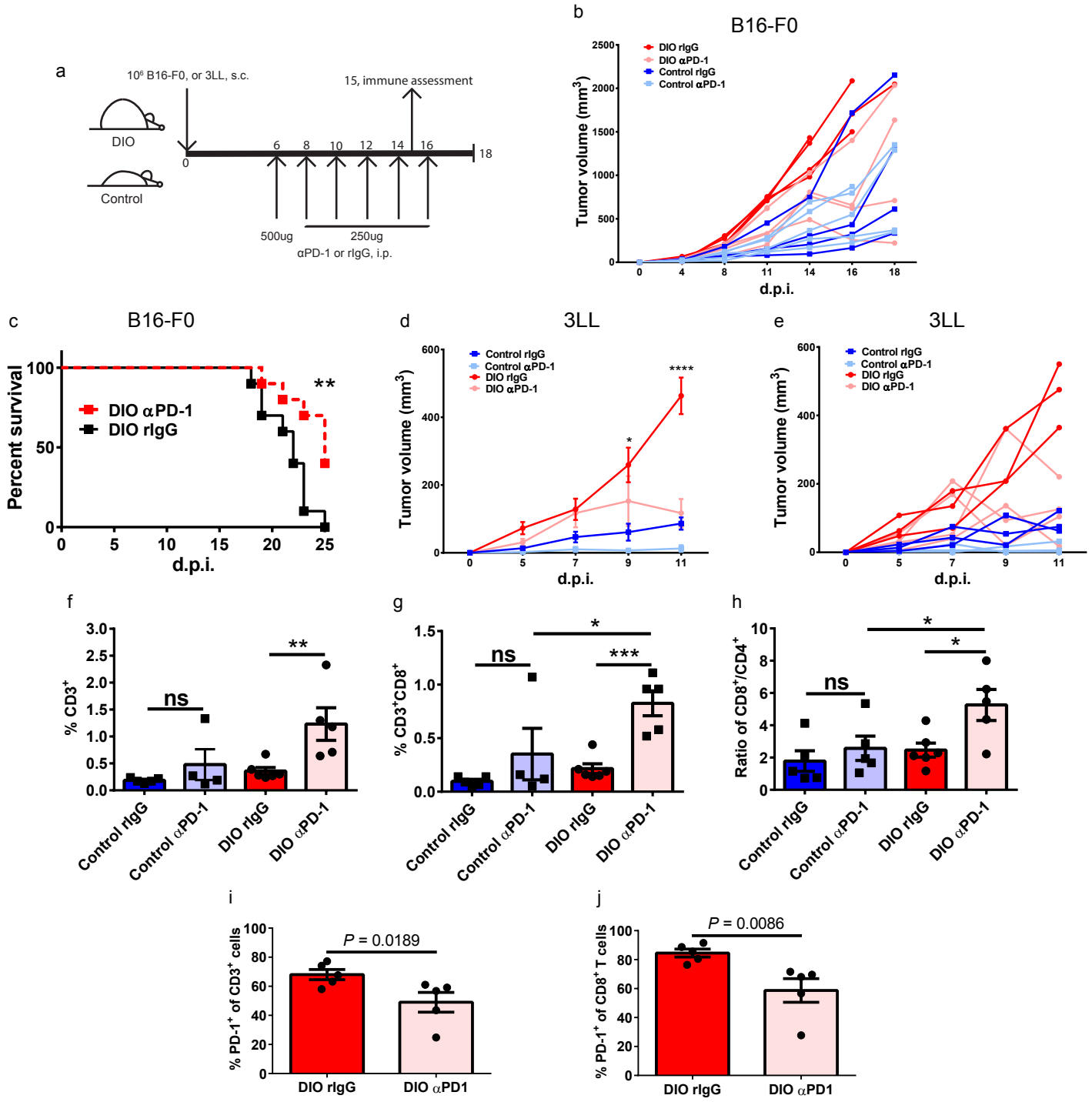


**Supplementary Figure 13: αPD-1 therapy in tumor-bearing control and DIO mice.** a) Schema of tumor implantation and αPD-1 therapy in control and DIO mice. b) Individual tumor volumes of B16-F0 melanoma in 6-month-old control and DIO C57BL/6 male mice (n=4 in control and DIO rIgG groups, n=5 in control and DIO αPD-1 groups). c) Kaplan-Meier survival curves are shown to compare B16-F0-tumor-bearing control and DIO mice treated with or without αPD-1 (n=10/group). Log-rank (Mantel-Cox) test used to compare groups. d) Tumor volume of 3LL inoculated subcutaneously in 6-month-old control and DIO C57BL/6 male mice treated with or without αPD-1 (n=3 in control rIgG, αPD-1 and DIO rIgG groups, n=4 in DIO αPD-1 group). Tumor volumes are depicted as mean ±s.e.m. Two-way ANOVA with Tukey post-hoc test used to compare groups. e) Individual tumor volumes of 3LL tumors in 6-month-old control and DIO C57BL/6 male mice treated with or without αPD-1. Frequency of f) CD3+ and g) CD3+CD8+ cells in the tumors of B16-F0-bearing control and DIO mice treated with or without αPD-1 (n=6 in DIO rIgG group, n=5 in control rIgG and DIO αPD-1 groups, n=4 in control αPD-1 group). h) The ratio of tumor-infiltrating CD8+ to CD4+ T cells in the tumors of B16-F0-bearing control and DIO mice treated with or without αPD-1 (n=6 in DIO rIgG group, n=5 in control rIgG, αPD-1 and DIO αPD-1 groups). f-h) Data are depicted as mean ±s.e.m., with all individual points shown. One-way ANOVA with Tukey post-hoc test used to compare groups. Frequency of PD-1 expression on i) CD3+ and j) CD8+ T cells in the tumors of DIO mice with and without αPD-1 treatment (n=5/group). Data are depicted as mean ±s.e.m., with all individual points shown. One-tailed unpaired Student's t-test *p<0.05, **p<0.01, ***p<0.005, ****p<0.001.

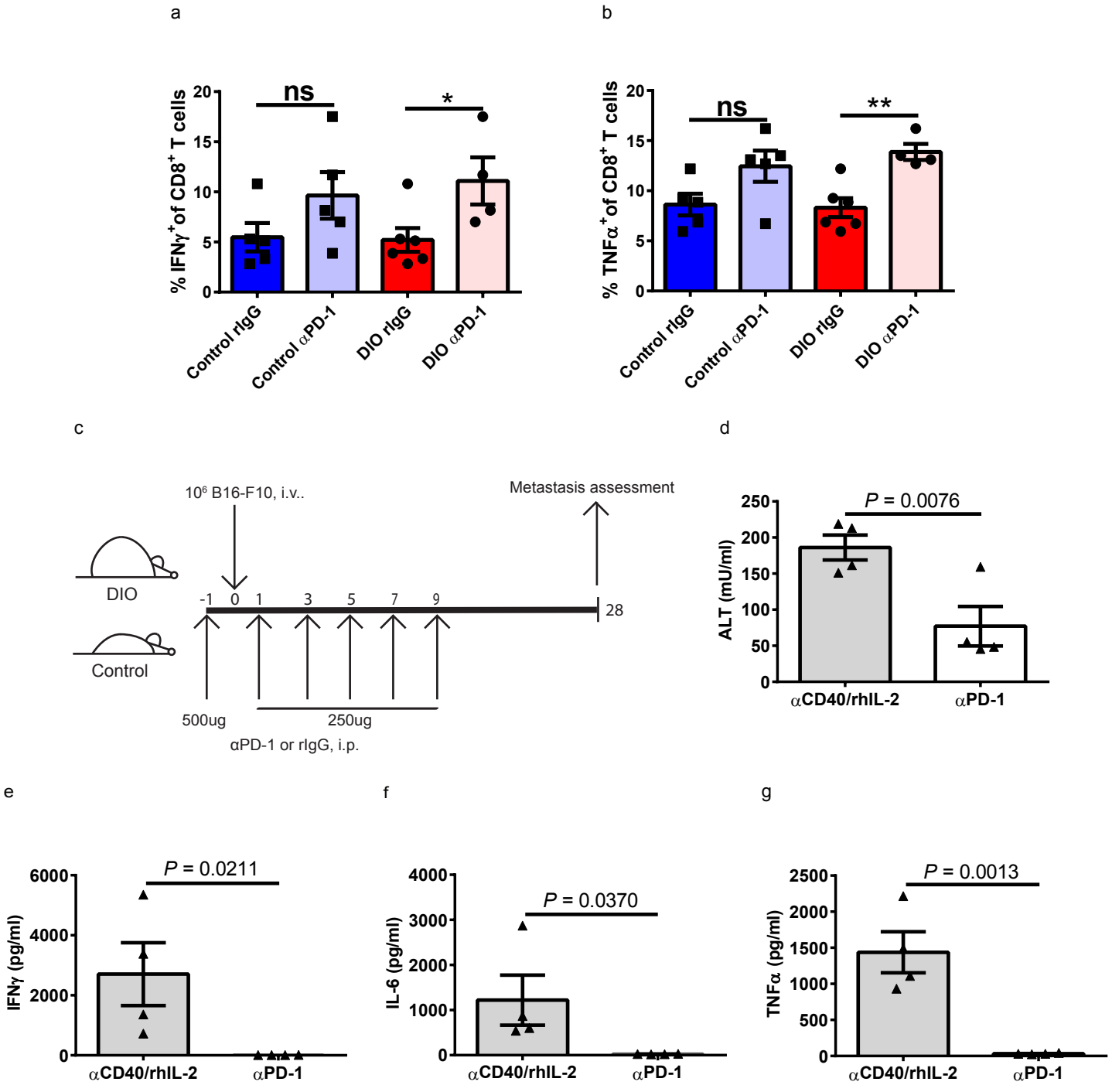


**Supplementary Figure 14: αPD-1 treatment reinvigorates T cell function with less toxicity in tumor-bearing DIO mice.** Frequency of a) IFNγ and b) TNFα producing CD8+ splenic T cells from tumor-bearing control and DIO mice after ex vivo stimulation (n=6 in DIO rIgG group, n=5 in control rIgG and αPD-1 groups, n=4 in DIO αPD-1 group). Data are depicted as mean ±s.e.m., with all individual points shown. One-way ANOVA with Tukey post-hoc test used to compare groups. c) Schema of systemic B16-F10 implantation and αPD-1 therapy in 6-month-old control and DIO male mice. The levels of d) ALT, e) IFNγ, f) IL-6 and g) TNFα in the serum of B16-F0-bearing DIO mice which were treated with either αCD40/rhIL-2 or αPD-1. Data are depicted as mean ±s.e.m., with all individual points shown. One-tailed unpaired Student's t-test used to compare groups. *p<0.05, **p<0.01.

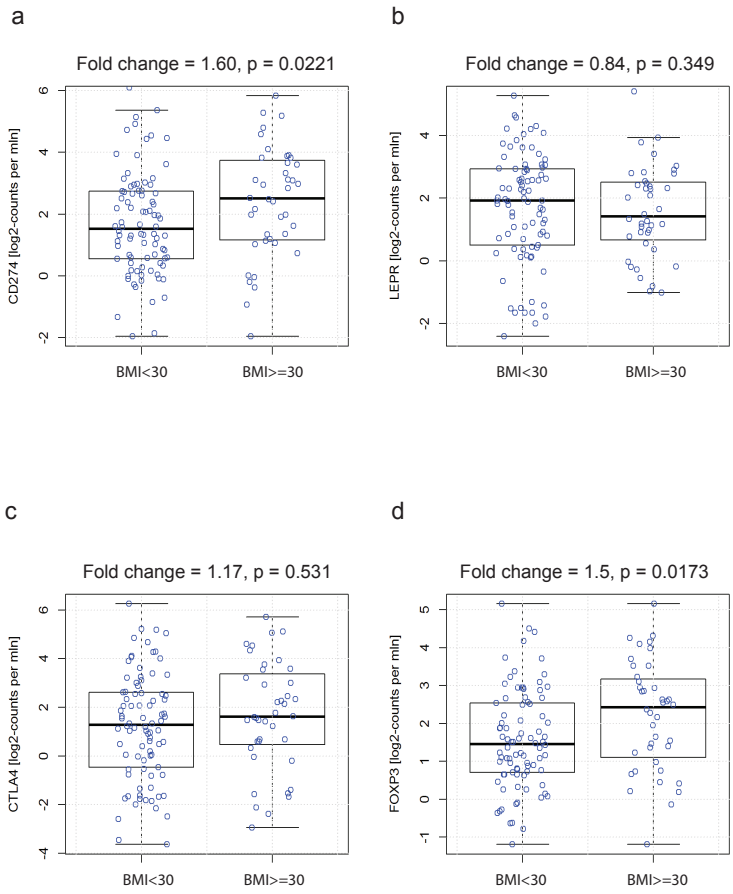


**Supplementary Figure 15: Immune exhaustion profiles of cancer patients.** Human TCGA data analysis of a) CD274 (PD-L1), b) LEPR, c) CTLA4, and d) FOXP3 expression in melanoma tumors from non-obese (n=86) vs. obese (n=40) patients. The line within each notch box represents the median. The lower and upper boundaries of the box indicate first and third quartiles respectively. The whiskers indicate the minimum and maximum values. P-value was calculated via DESeq2 (Wald-Test) to compare groups.

Supplementary Table 1. Healthy donor patient characteristics

| Age | Sex | BMI |
|---|---|---|
| 35 | F | 18.8 |
| 37 | F | 18.9 |
| 33 | F | 20 |
| 32 | F | 20.8 |
| 40 | F | 21.3 |
| 27 | F | 21.3 |
| 31 | F | 22.2 |
| 58 | F | 22.3 |
| 38 | F | 22.5 |
| 29 | F | 30.2 |
| 28 | F | 31.4 |
| 37 | F | 34.8 |
| 60 | F | 34.8 |
| 35 | F | 35.2 |
| 53 | F | 36.2 |
| 41 | F | 36.9 |
| 27 | F | 38.1 |
| 54 | F | 38.5 |
| 52 | F | 41.6 |
| 27 | F | 42.6 |
| 43 | F | 50.6 |
| **BMI<30: Mean age: 38 +/- 10<br>BMI≥30: Mean age: 44 +/- 13<br>p=0.46** | | |

Supplementary Table 2. Patient characteristics and irAE

| Variable | Overall (n=250) | BMI < 30 (n=169) | BMI ≥ 30 (n=81) |
|---|---|---|---|
| **BMI Mean (SD)** | 27.4 (7.3) | 23.4 (3.6) | 35.7 (6.2) |
| **BMI Range** | 15 -56.6 | 15 - 29.9 | 30.0 - 56.6 |
| **Age Mean (SD)** | 61.7 (13.7) | 62.6 (14.6) | 59.70 (11.52) |
| **Age Range** | 23, 91 | 23, 91 | 36, 87 |
| **Sex** | | | |
| **M (%)** | 114 (45.6) | 80 (47.3) | 34 (42.0) |
| **F (%)** | 138 (54.4) | 89 (52.7) | 47 (58.0) |
| **Cancer Type** | | | |
| **Lung (%)** | 55 (22.0) | 44 (26.0) | 11 (13.6) |
| **Melanoma (%)** | 45 (18.0) | 23 (13.6) | 22 (27.2) |
| **Ovarian (%)** | 20 (8.0) | 17 (10.1) | 3 (3.7) |
| **Other (%)** | 130 (52.0) | 85 (50.3) | 45 (55.6) |
| **ECOG** | | | |
| **0 (%)** | 70 (28.00) | 48 (28.4) | 22 (27.2) |
| **1 (%)** | 134 (53.6) | 87 (51.5) | 47 (58.0) |
| **2 or More (%)** | 46 (18.4) | 34 (20.1) | 12 (14.8) |
| **Prior Therapy** | | | |
| **1 (%)** | 44 (17.6) | 24 (14.2) | 20 (24.7) |
| **2 (%)** | 91 (36.4) | 66 (39.1) | 25 (30.9) |
| **3 or More (%)** | 115 (46.0) | 79 (46.7) | 36 (44.4) |
| **irAE (%)** | 52 (20.8) | 32 (18.9) | 20 (24.7) |
| **irAE type** | | | |
| **Colitis** | 23 | 13 | 10 |
| **Pnuemonitis** | 11 | 8 | 3 |
| **Thyroid** | 14 | 9 | 5 |
| **Colitis + Thyroid** | 4 | 2 | 2 |

Supplementary Table 3. Details of flow cytometry antibodies.

| *Name* | *Vendor* | *Cat#* | *Fluorochrome* | *Clone #* | *Dilution (for 50ul)* | *Validation* | *Reference* |
|---|---|---|---|---|---|---|---|
| CD45 | Biolegend | 103126 | PB | 30-F11 | 200 | https://www.biolegend.com/en-us/products/pacific-blue-anti-mouse-cd45-antibody-3102 | Jiang Q, et al. 2008. Blood. 112:2858 |
| CD45 | Biolegend | 103116 | APC-Cy7 | 30-F11 | 200 | https://www.biolegend.com/en-us/products/apc-cy7-anti-mouse-cd45-antibody-2530 | Krasteva G, et al. 2011. Proc Natl Acad Sci U S A. 108:9478 |
| CD44 | Biolegend | 103020 | PB | IM7 | 100 | https://www.biolegend.com/en-us/products/pacific-blue-anti-mouse-human-cd44-antibody-3099 | Lee JW, et al. 2006. Nature Immunol. 8:181. |
| CD4 | Biolegend | 100550 | BV711 | RM4-5 | 200 | https://www.biolegend.com/en-us/products/brilliant-violet-711-anti-mouse-cd4-antibody-7925 | Shigeta A, et al. 2008. Blood 112:4915. |
| CD8a | Biolegend | 100744 | BV605 | 53-6.7 | 320 | https://www.biolegend.com/en-us/products/brilliant-violet-605-anti-mouse-cd8a-antibody-7636 | Ko SY, et al. 2005. J. Immunol. 175:3309. |
| CD3 | Biolegend | 100232 | BV785 | 17A2 | 40 | https://www.biolegend.com/en-us/products/brilliant-violet-785-anti-mouse-cd3-antibody-7953 | Lofano G, et al. 2015. J Immunol. 195: 1617-1627. |
| TNFα | Biolegend | 506324 | PE-Cy7 | MP6-XT22 | 80 | https://www.biolegend.com/en-us/products/pe-cy7-anti-mouse-tnf-alpha-antibody-5866 | Lawson BR, *et al.* 2007. *J. Immunol.* 178:5366 |
| Ki67 | Biolegend | 652420 | Alexa Fluor 700 | 16A8 | 400 | https://www.biolegend.com/en-us/products/alexa-fluor-700-anti-mouse-ki-67-antibody-10366 | Guillaumond F, *et al.* 2015. *PNAS.* 112:2473 |
| T-bet | Biolegend | 644804 | Alexa Fluor 647 | 4B10 | 50 | https://www.biolegend.com/en-us/products/alexa-fluor-647-anti-t-bet-antibody-5759 | Feng J,et al. 2017. Nat Commun. 10.1038/s41467-017-01056-8 |
| CD279 (PD-1) | ebioscience/ThermoFisher | 11-9981-82 | FITC | RMP1-30 | 50 | https://www.thermofisher.com/antibody/product/CD279-PD-1-Antibody-clone-RMP1-30-Monoclonal/11-9981-82 | Starobinets H, et al. 2016. JCI. 1;126(12):4417-4429. doi: 10.1172/JCI85705 |
| FoxP3 | ebioscience/ThermoFisher | 11-5773-80 | FITC | FJK-16s | 100 | https://www.thermofisher.com/antibody/product/FOXP3-Antibody-clone-FJK-16s-Monoclonal/11-5773-82 | Liu Z, et al. 2017. Nat Commun. 27;8:14754. doi: 10.1038/ncomms14754 |
| Eomes | ebioscience/ThermoFisher | 61-4875-82 | PE-eFluor 610 | Dan11mag | 50 | https://www.thermofisher.com/antibody/product/EOMES-Antibody-clone-Dan11mag-Monoclonal/61-4875-82 | Wang H, et al. 2017. Int J Med Sci. 18;14(10):977-983. doi: 10.7150/ijms.20212. eCollection 2017 |
| Tim3 | ebioscience/ThermoFisher | 12-5870-82 | PE | RMT3-23 | 80 | https://www.thermofisher.com/antibody/product/CD366-TIM3-Antibody-clone-RMT3-23-Monoclonal/12-5870-82 | Kim DS, et al. 2017. Nat Commun. 24;8(1):344. doi: 10.1038/s41467-017-00324-x. |
| CD223 (Lag3) | ebioscience/ThermoFisher | 46-2231-82 | PerCP-ef710 | eBioC9B7W | 80 | https://www.thermofisher.com/antibody/product/CD223-LAG-3-Antibody-clone-eBioC9B7W-C9B7W-Monoclonal/46-2231-82 | Di Marco Barros R, et al, 2016. Cell. 22;167(1):203-218.e17. doi: 10.1016/j.cell.2016.08.030. Epub 2016 Sep 15 |
| CD62L | ebioscience/ThermoFisher | 25-0621-82 | PE-Cy7 | MEL-14 | 160 | https://www.thermofisher.com/antibody/product/CD62L-L-Selectin-Antibody-clone-MEL-14-Monoclonal/25-0621-82 | Deng R, et al, Nat Commun. 17;8(1):978. doi: 10.1038/s41467-017-00880-2 |
| CD274 (PD-L1)(B7-H1) | ebioscience/ThermoFisher | 12-5982-83 | PE | MIH5 | 50 | https://www.thermofisher.com/antibody/product/CD274-PD-L1-B7-H1-Antibody-clone-MIH5-Monoclonal/12-5982-82 | Tian Y, et al, Immunity. 17;44(5):1204-14. doi: 10.1016/j.immuni.2016.04.008. Epub 2016 May 3. |
| pSTAT3 | ebioscience/ThermoFisher | 17-9033-42 | APC | LUVNKLA | 40 | https://www.thermofisher.com/antibody/product/Phospho-STAT3-Tyr705-Antibody-clone-LUVNKLA-Monoclonal/17-9033-42 | |
| IFNγ | BD Biosciences | 561479 | APC-Cy7 | XMG1.2 | 80 | http://www.bdbiosciences.com/us/applications/research/t-cell-immunology/th-1-cells/intracellular-markers/cytokines-and-chemokines/mouse/apc-cy7-rat-anti-mouse-ifn--xmg12/p/561479 | Cherwinski HM, et al. J Exp Med. 1987; 166(5):1229-1244 |
| CD3 | BD | 558124 | PacBlue | SP34-2 | 167 | http://www.bdbiosciences.com/us/reagents/research/antibodies-buffers/immunology-reagents/anti-non-human-primate-antibodies/cell-surface-antigens/pacific-blue-mouse-anti-human-cd3-sp34-2/p/558124 | Carter DL, Shieh TM, Blosser RL et al. CD56 identifies monocytes and not natural killer cells in rhesus macaques. Cytometry. 1999; 37(1):41-50. |
| CD4 | BD | 562843 | BV605 | L200 | 50 | http://www.bdbiosciences.com/us/reagents/research/antibodies-buffers/immunology-reagents/anti-non-human-primate-antibodies/cell-surface-antigens/bv605-mouse-anti-human-cd4-l200/p/562843 | Giorgi JV, Hultin LE, Desrosiers RC. The immunopathogenesis of retroviral diseases: no immunophenotypic alterations in T, B, and NK cell subsets in SIVmac239-challenged rhesus macaques protected by SIV delta nef vaccination. J Med Primatol. 1996; 25(3):186-191. |
| CD8 | BD | 557945 | AF700 | RPA-T8 | 50 | http://www.bdbiosciences.com/us/reagents/research/antibodies-buffers/immunology-reagents/anti-human-antibodies/cell-surface-antigens/alexa-fluor-700-mouse-anti-human-cd8-rpa-t8/p/557945 | Reimann KA, Waite BC, Lee-Parritz DE, et al. Use of human leukocyte-specific monoclonal antibodies for clinically immunophenotyping lymphocytes of rhesus monkeys. Cytometry. 1994; 17(1):102-108. |
| CD95 | BD | 558814 | APC | DX2 | 50 | http://www.bdbiosciences.com/us/applications/research/t-cell-immunology/regulatory-t-cells/surface-markers/human/apc-mouse-anti-human-cd95-dx2/p/558814 | Villinger, F., Bostik, P., Mayne, A., King, C. L., Genain, C. P., Weiss, W. R., & Ansari, A. A. (2001). Cloning, sequencing, and homology analysis of nonhuman primate Fas/Fas-ligand and co-stimulatory molecules. *Immunogenetics* , *53* (4), 315-328. |
| CD28 | BD | 561368 | APC-H7 | CD28.2 | 10 | https://www.bdbiosciences.com/us/applications/research/t-cell-immunology/regulatory-t-cells/surface-markers/human/apc-h7-mouse-anti-human-cd28-cd282/p/561368 | Page, A., Srinivasan, S., Singh, K., Russell, M., Hamby, K., Deane, T., ... & Strobert, E. (2012). CD40 blockade combines with CTLA4Ig and sirolimus to produce mixed chimerism in an MHC defined rhesus macaque transplant model. *American Journal of Transplantation* , *12* (1), 115-125. |
| PD-1 | Biolegend | 329906 | PE | EH12.2H7 | 50 | https://www.biolegend.com/en-us/products/pe-anti-human-cd279-pd-1-antibody-4412 | Xu, H., Wang, X., Lackner, A. A., & Veazey, R. S. (2014). PD-1HIGH follicular CD4 T helper cell subsets residing in lymph node germinal centers correlate with B cell maturation and IgG production in rhesus macaques. *Frontiers in immunology* , *5* , 85. |
| Ki-67 | BD | 561165 | AF488 | B56 | 50 | http://www.bdbiosciences.com/us/applications/research/apoptosis/conjugated-antibodies/alexa-fluor-488-mouse-anti-ki-67-b56/p/561165 | Pitcher CJ, Hagen SI, Walker JM, et al. Development and homeostasis of T cell memory in rhesus macaque. J Immunol. 2002; 168(1):29-43. |
| Live/Dead | invitrogen | L34966 | Aqua | n/a | 50 | https://www.thermofisher.com/order/catalog/product/L34966 | Lugli, E., Gattinoni, L., Roberto, A., Mavilio, D., Price, D. A., Restifo, N. P., & Roederer, M. (2013). Identification, isolation and in vitro expansion of human and nonhuman primate T stem cell memory cells. *Nature protocols* , *8* (1), 33. |